Phonon band structure and thermal transport correlation in a layered diatomic crystal

A. J. H. McGaughey* and M. I. Hussein†
Department of Mechanical Engineering, University of Michigan, Ann Arbor, Michigan 48109-2125, USA

E. S. Landry
Department of Mechanical Engineering, Carnegie Mellon University, Pittsburgh, Pennsylvania 15213-3890, USA

M. Kaviany and G. M. Hulbert
Department of Mechanical Engineering, University of Michigan, Ann Arbor, Michigan 48109-2125, USA
(Received 2 June 2006; published 29 September 2006)

To elucidate the three-way relationship among a crystal's structure, its phonon dispersion characteristics, and its thermal conductivity, an analysis is conducted on layered diatomic Lennard-Jones crystals with various mass ratios. Lattice dynamics theory and molecular dynamics simulations are used to predict the phonon dispersion curves and the thermal conductivity. The layered structure generates directionally dependent thermal conductivities lower than those predicted by density trends alone. The dispersion characteristics are quantified using a set of band diagram metrics, which are used to assess the contributions of acoustic phonons and optical phonons to the thermal conductivity. The thermal conductivity increases as the extent of the acoustic modes increases, and it decreases as the extent of the stop bands increases. The sensitivity of the thermal conductivity to the band diagram metrics is highest at low temperatures, where there is less anharmonic scattering, indicating that dispersion plays a more prominent role in thermal transport in that regime. We propose that the dispersion metrics (i) provide an indirect measure of the relative contributions of dispersion and anharmonic scattering to the thermal transport, and (ii) uncouple the standard thermal conductivity structure-property relation to that of structure-dispersion and dispersion-property relations, providing opportunities for better understanding of the underlying physical mechanisms and a potential tool for material design.

DOI: 10.1103/PhysRevB.74.104304 PACS number(s): 63.20.Dj

I. INTRODUCTION

Thermal transport in a dielectric crystal is governed by phonon dispersion and phonon scattering.[1] The majority of theoretical studies of thermal transport in dielectrics deal with phonon dispersion at a qualitative level. A common treatment is to assume that the contribution of optical phonons to the thermal conductivity is negligible because the associated dispersion branches are often flat, implying low phonon group velocities. Theories that quantitatively relate dispersion characteristics to bulk thermal transport properties are limited. One example is the use of phonon dispersion curves to determine the phonon group and phase velocities required in the single mode relaxation time formulation of the Boltzmann transport equation (BTE).[2,3] Even in such a case, the dispersion is usually greatly simplified. The importance of accurately and completely incorporating dispersion into this BTE formulation has recently been investigated for bulk materials[4,5] and for nanostructures.[6,7]

Dong *et al.*[8] report evidence of the important role that phonon dispersion plays in thermal transport in their study of germanium clathrates using molecular dynamics (MD) simulations. In their Fig. 1, they show phonon dispersion curves for a diamond structure, a clathrate cage, and the same cage structure but filled with weakly bonded guest strontium atoms that behave as "rattlers." Although the range of frequencies accessed by the vibrational modes in these three structures is comparable, the dispersion characteristics are quite different. The large unit cell of the clathrate cage significantly reduces the frequency range of the acoustic phonons, the carriers generally assumed to be most responsible for thermal transport. There is an accompanying factor of 10 reduction in the thermal conductivity. In the filled cage, the encapsulated guest atoms have a natural frequency that cuts directly through the middle of what would be the acoustic phonon branches, and the value of the thermal conductivity is reduced by a further factor of 10. Experimental studies on filled cagelike structures have found similar results, i.e., that rattler atoms can reduce the thermal conductivity.[9,10]

Considering phonon dispersion is also important in studying thermal transport in superlattices.[11–14] Using an inelastic phonon Boltzmann approach to model anharmonic three-phonon scattering processes, Broido and Reinecke[11] studied the thermal conductivity of a model two-mass superlattice with a diamond structure, and how it depends on the mass ratio and layer thickness. As the mass ratio is increased, the dispersion curves flatten, which tends to lower the thermal conductivity. At the same time, the increase in mass ratio reduces the cross-section for Umklapp scattering, which tends to increase the thermal conductivity. The relative importance of these two mechanisms is found to be a function of the layer thickness. Using a kinetic theory model, Simkin and Mahan[12] found that as the layer thickness in a model superlattice is reduced, the thermal conductivity decreases due to an increase in ballistic scattering stemming from the rise in interface density. It was shown in the same study that as the layer thickness is further reduced to values sufficiently smaller than the phonon mean free path, the thermal conductivity increases. This transition, which predicts a minimum superlattice thermal conductivity, was attributed to a shift from phonon transport best described by a particle theory to one that follows a wave theory. This minimum superlattice

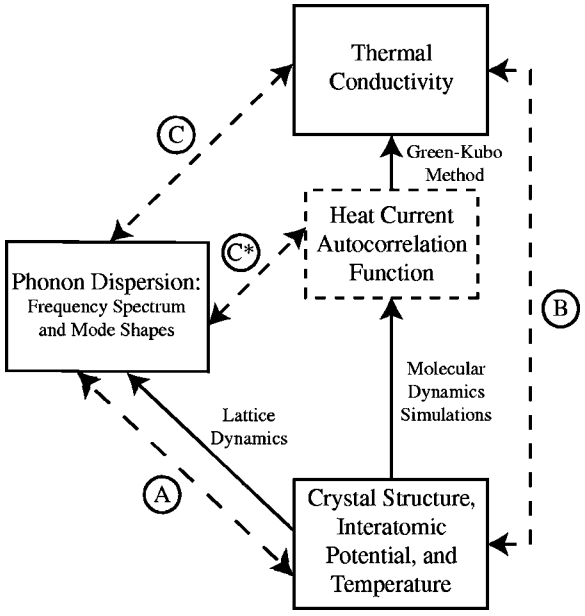

FIG. 1. Schematic of the relationships among atomic structure, dispersion characteristics, and thermal conductivity. Shown are both the tools available for moving between these blocks (solid lines) and the links we are seeking to establish (dashed lines). Link A is discussed in Sec. III, link B in Sec. IV C, link C* in Sec. V A and link C in Sec. V B. In this investigation, we restrict our discussion of the lattice dynamics to the phonon mode frequencies.

thermal conductivity has also been measured in experiments[15–17] and predicted in MD simulations.[13] The need for a wave treatment of phonons indicates that interference mechanisms affect the phonon transport.

Apart from the above-mentioned efforts, few investigations have attempted to rigorously establish a connection between dispersion characteristics, which include the size and location of frequency pass bands (and stop bands), and thermal transport properties. In this work we explore the three-way relationship in a crystal between: (i) the unit cell structure, (ii) the associated dispersion characteristics, and (iii) the bulk thermal transport behavior, using lattice dynamics calculations and MD simulations, as shown in Fig. 1. The dispersion characteristics are quantified using a set of frequency band diagram metrics. As a starting point, we narrow our attention to a diatomic Lennard-Jones (LJ) crystal that corresponds to a monolayer superlattice. The atomic species are only differentiated by their masses. By modeling a simple system, phenomena can be observed that might not be discernable in more complex structures. The overall theme of the investigation, however, is intended for dielectric crystals in general, and the analysis tools developed are not limited to superlattices.

The insights gained in this study could lead to the development of a systematic technique for the atomic-level design of materials with desired thermal transport properties. This capability could facilitate the introduction of new, yet realizable, materials with very high or low thermal conductivities. Examples of applications include thermoelectric materials with high figure-of-merit, microelectronic devices enjoying enhanced cooling characteristics, and efficient thermal insulators for chemical processing.

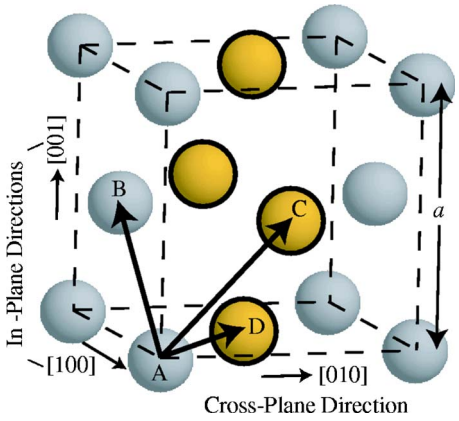

FIG. 2. (Color online) The four-atom unit cell of the layered diatomic crystal. If the four atoms are equivalent, the crystal structure is fcc. If A and B have a different mass than C and D, the crystal structure is simple cubic. The arrangement chosen leads to planes with a thickness of one atomic layer stacked in the [010] (cross-plane) direction.

We begin by presenting the diatomic crystal structure and basic information pertaining to the MD simulations. Phonon dispersion relations are then determined using lattice dynamics calculations and analyzed for different mass ratios at various temperatures. The band diagram metrics are introduced and discussed. We then use MD simulations and the Green-Kubo (GK) method to predict the thermal conductivities of these structures. Discussion is presented with regard to the magnitude of the thermal conductivity, its directional and temperature dependencies, and its relation to the unit cell. We then explore the relationship between the thermal conductivity and the associated dispersion band structure.

II. CRYSTAL STRUCTURE AND MOLECULAR DYNAMICS SIMULATIONS

We perform our study of the relationship among atomic structure, phonon band structure, and thermal transport by considering model systems described by the LJ potential,

$$\phi_{ij}(r_{ij}) = 4\epsilon_{\mathrm{LJ}}\left[\left(\frac{\sigma_{\mathrm{LJ}}}{r_{ij}}\right)^{12} - \left(\frac{\sigma_{\mathrm{LJ}}}{r_{ij}}\right)^{6}\right]. \quad (1)$$

Here, ϕ_{ij} is the potential energy associated with a pair of particles (i and j) separated by a distance r_{ij}, the potential well depth is ϵ_{LJ}, and the equilibrium pair separation is $2^{1/6}\sigma_{\mathrm{LJ}}$. The LJ potential is commonly used in investigations of thermal transport in bulk and composite systems.[5,13,14,18–23] Dimensional quantities have been scaled for argon, for which ϵ_{LJ} and σ_{LJ} have values of 1.67×10^{-21} J and 3.4×10^{-10} m.[24] The argon mass scale, m_{LJ}, is 6.63×10^{-26} kg (the mass of one atom). Quantities reported in dimensionless LJ units are indicated by an asterisk.

The structure we consider is a simple-cubic crystal with a four-atom basis (unit cell) and lattice parameter a, as shown in Fig. 2. If the four atoms A–D are identical, the conventional unit-cell representation of the face-centered-cubic (fcc) crystal structure is obtained. By taking two of the atoms in

the basis (A, B) to have one mass, m_1, and the other two (C, D) to have a different mass, m_2, a crystal with alternating layers of atoms in the [010] direction [which we will refer to as the cross-plane (CP) direction] is created. We will refer to the [100] and [001] directions as the in-plane (IP) directions. This structure is a monolayer superlattice. The value of m_2 is fixed at m_{LJ}, and the mass ratio R_m is defined as

$$R_m \equiv \frac{m_1}{m_2}. \tag{2}$$

The dimensionless mass of the atoms in a monatomic system will be denoted by m^*. It has a value of unity, unless noted. By varying only the atomic masses, the LJ potential can be applied to this system without any modification. We primarily consider R_m values of 1 (the monatomic unit cell), 2, 5, and 10. We note that this variation in atomic masses is in the same spirit as the work of Broido and Reinecke[11] and Che *et al.*,[25] who considered two-mass diamond systems.

The MD simulations are performed in dimensionless LJ units. All results can be scaled to dimensional values using the parameters ϵ_{LJ}, σ_{LJ}, and m_{LJ}, and the Boltzmann constant, k_{B}, which is part of the temperature scale, $\epsilon_{\mathrm{LJ}}/k_{\mathrm{B}}$. From dimensional analysis, it can be shown that the thermal conductivity of the $1/R_m$ system, k_{1/R_m}, is related to that of the R_m system, k_{R_m}, through

$$k_{1/R_m} = k_{R_m} R_m^{1/2}. \tag{3}$$

Thus, one dimensionless simulation can be used to generate data for both the R_m system and the $1/R_m$ system. Where helpful, data corresponding to mass ratios of 0.1, 0.2, and 0.5 will be presented.

The purpose of the MD simulations is (i) to obtain the zero-pressure lattice parameter as a function of temperature (used in later simulations and for lattice dynamics calculations) and (ii) to predict the thermal conductivity. Because the functional form of the LJ potential is kept the same (we consider only different masses), the zero-pressure unit cell parameters remain unchanged from those for a single-mass system.[5]

All reported MD results are generated from simulations run in the *NVE* (constant mass, volume, and energy) ensemble at zero pressure with a time step of 4.285 fs. The simulation cell contains 512 atoms (eight unit cells in the cross-plane direction and four in the in-plane direction) and periodic boundary conditions are imposed in all three directions. This system size was found to be sufficient to obtain computational domain size-independent thermal conductivities. The MD procedures have been described in detail elsewhere.[5,22,26] We consider temperatures T between 10 and 80 K in 10 K increments. The melting temperature of the monatomic system is 87 K. The data presented in the thermal conductivity analysis for a given parameter set (R_m, T, and the crystallographic direction) are obtained by averaging over five independent simulations so as to get a representative sampling of the associated phase space. In each of the five simulations, information is obtained over 1×10^6 time steps, after an equilibration period of 5×10^5 time steps.

III. PHONON DISPERSION

The frequency (phonon) space characteristics of a solid phase can be determined with lattice dynamics calculations,[27] in which the real-space coordinates (the positions) are transformed into the normal mode coordinates (the phonon modes). Each normal mode has a frequency, ω, wave vector, $\boldsymbol{\kappa}$, and polarization vector, $\mathbf{e}$ (which describes the mode shape). The available wave vectors are obtained from the crystal structure, and the frequencies and polarization vectors are found by solving the eigenvalue equation[27]

$$\omega^2(\boldsymbol{\kappa},\nu)\mathbf{e}(\boldsymbol{\kappa},\nu) = \mathbf{D}(\boldsymbol{\kappa})\cdot\mathbf{e}(\boldsymbol{\kappa},\nu), \tag{4}$$

where $\mathbf{D}(\boldsymbol{\kappa})$ is the dynamical matrix for the unit cell and the parameter ν identifies the polarization for a given wave vector. The lattice dynamics methods used are reviewed in the Appendix.

The predictions of harmonic lattice dynamics calculations from Eq. (4) at zero temperature are exact and can be found using the equilibrium atomic positions and the interatomic potential. As the temperature rises, the system will move away from the zero-temperature minimum of the potential energy surface. The lattice dynamics are affected in two ways. First, the solid will either expand or contract. This effect can be accounted for by using the finite-temperature lattice constant in the harmonic lattice dynamics formulation (the quasi-harmonic approximation).[27] Second, the motions of the atoms will lead to anharmonic interactions. These effects cannot be easily accounted for in the formal lattice dynamics theory due to the difficulty in incorporating third-order (and higher) derivatives of the interatomic potential. In an MD simulation, it is possible, with considerable effort, to capture the true anharmonic lattice dynamics.[5] For the purposes of this investigation, however, we restrict the analysis to the quasi-harmonic formulation. Further discussion of this choice will follow where appropriate.

We now consider the relationship between the mass ratio R_m and the dispersion characteristics (A in Fig. 1) by plotting a set of dispersion curves in Figs. 3(a)–3(c). The plots in Fig. 3 are of dimensionless frequency, $\omega^* = \omega/(\epsilon_{\mathrm{LJ}}/m_{\mathrm{LJ}}\sigma_{\mathrm{LJ}}^2)^{1/2}$, vs dimensionless wave number, defined as $\kappa^* = \kappa/(2\pi/a)$. The zero-temperature phonon dispersion curves for the monatomic ($R_m=1$) unit cell in the [100] direction are shown in Fig. 3(a). As this system has cubic isotropy, the dispersion characteristics are the same for the [010] and [001] directions. For the monatomic crystal, the true Brillouin zone extends to a κ^* value of unity in the [100] direction and is a truncated octahedron. Here, to be consistent with the plots for the layered structure (where the Brillouin zone extends to a κ^* value of 0.5 and is cubic), the branches have been folded over at their midpoints.

The zero-temperature dispersion curves for the in-plane and cross-plane directions for the $R_m=10$ unit cell are shown in Figs. 3(b) and 3(c). The anisotropy of the crystal structure is reflected in the directional dependence of the plotted dispersion curves. At nonunity mass ratios, stop bands (band gaps) in the frequency spectra are evident and grow as R_m is increased. A stop band in the in-plane direction opens when

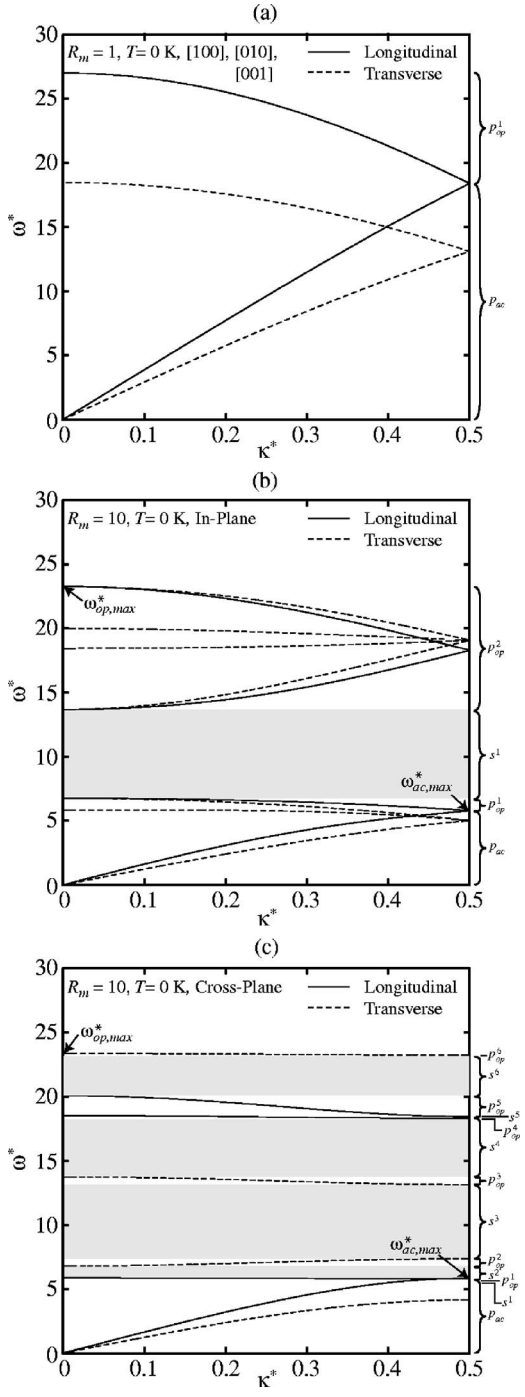

FIG. 3. (a) Phonon dispersion curves for the monatomic crystal. The dispersion characteristics are the same in the [100], [010], and [001] directions. All branches correspond to acoustic phonons, and have been folded over at $\kappa^*=0.5$. Phonon dispersion curves for $R_m=10$: (b) in-plane and (c) cross-plane directions. The maximum acoustic and optical frequencies are noted, and the stop bands are shaded.

the mass ratio is 1.17 and in the cross-plane direction when the mass ratio is 1.62. The stop bands in Figs. 3(b) and 3(c) are shaded gray.

The dispersion curves plotted correspond to a crystal of infinite size and are thus continuous. Because of the finite size of the simulation cell, only the modes at κ^* values of 0, 0.25, and 0.5 will be present in the MD simulations for the in-plane directions, and at κ^* values of 0, 0.125, 0.25, 0.375, and 0.5 for the cross-plane direction.

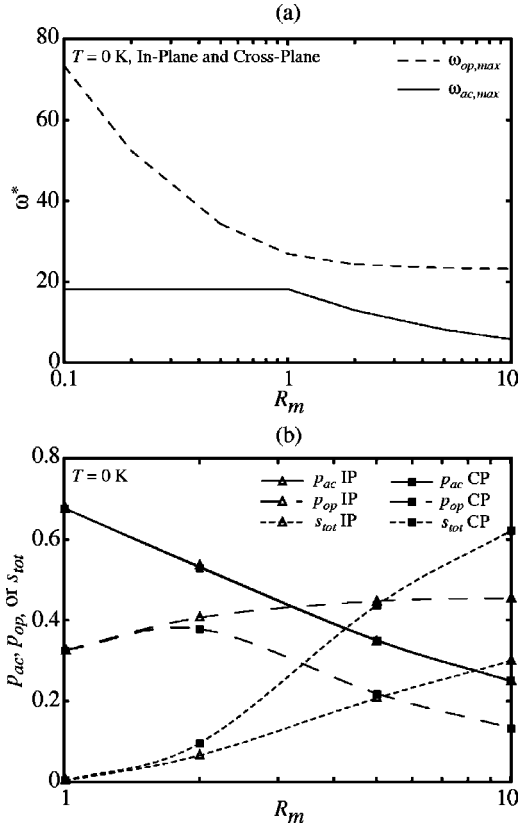

FIG. 4. (a) Maximum frequencies of the acoustic and optical branches plotted against the mass ratio R_m at zero temperature. The data in the in-plane and cross-plane directions are indistinguishable. (b) Breakdown of the frequency spectrum into the acoustic and optical pass bands (p_{ac} and p_{op}) and the stop bands, s_{all}. The p_{ac} curves for the two directions are indistinguishable. The data have been fit with smoothed curves to highlight the trends.

The maximum frequencies of the acoustic and optical branches at zero temperature are plotted in Fig. 4(a) for R_m values between 0.1 and 10. The data for the in-plane and cross-plane directions are indistinguishable. Maximum frequency values for the monatomic system are taken at κ^* values of 0.5 and 1 for the acoustic and optical branches. As the mass ratio is increased from unity, the maximum optical frequency decreases slightly and the maximum acoustic frequency decreases. As R_m is reduced below unity, the maximum optical frequency increases and the maximum acoustic frequency is essentially constant. The maximum optical frequency increases for small R_m because the lighter mass can oscillate at higher frequencies. These trends are qualitatively consistent with those predicted for a one-dimensional diatomic system.[28]

The LJ system expands as its temperature is raised, causing the phonon frequencies to decrease. At a temperature of 80 K, the quasi-harmonic dispersion calculations for the monatomic system give a maximum dimensionless frequency, $\omega^*_{op,max}$, of 16.6, compared to the zero-temperature maximum of 26.9. The temperature dependence of the maxi-

mum frequency is close to linear, and a similar percentage decrease is found for the nonunity mass ratios. The full anharmonic dispersion analysis for the monatomic system at a temperature of 80 K gives a maximum dimensionless frequency of 21.2.[5] The discrepancy between the quasi-harmonic and anharmonic dispersion curves increases with increasing temperature and wave vector magnitude. For the majority of the data considered here, the expected difference is $<10\%$, which we take to be satisfactory in lieu of calculating the full anharmonic dispersion characteristics.

In later analysis, we will investigate the relationship between thermal conductivity and the dispersion curves. To facilitate this analysis, we introduce three metrics for the dispersion curves: p_{ac}, p_{op}, and s_{all}. The idea of parametrizing the frequency band structure has previously been applied in the area of elastodynamics.[29] The first of the metrics, p_{ac}, is defined as the fraction of the frequency spectrum taken up by the acoustic branches, i.e., $p_{ac}=\omega_{ac,max}/\omega_{op,max}$. This is the acoustic-phonon pass band. Similarly, p_{op} represents the fraction of the spectrum taken up by the optical branches [the optical-phonon pass band(s)]. We calculate p_{op} as $\Sigma_i p_{op}^i$, where the summation is over the continuous ranges of the optical phonon bands, as shown in Figs. 3(b) and 3(c) (with appropriate normalization by $\omega_{op,max}$). The rest of the spectrum is made up of stop bands, whose contribution is given by $s_{all}=\Sigma_i s^i$, as shown in Figs. 3(b) and 3(c) (with appropriate normalization by $\omega_{op,max}$). Thus,

$$p_{ac}+p_{op}+s_{all}=1. \tag{5}$$

These three quantities are plotted as a function of the mass ratio for both the in-plane and cross-plane directions at zero temperature in Fig. 4(b). As the mass ratio increases, the acoustic phonons take up less of the spectrum (the results are essentially identical in the two directions), while the extent of the stop bands increases (more so in the cross-plane direction). The optical-phonon extent initially increases in both directions. This increase continues for the in-plane direction, but a decrease is found for the cross-plane direction, consistent with its larger stop band extent. The temperature dependence of p_{ac}, p_{op}, and s_{all} is small ($\sim 1\%$ change between temperatures of 0 and 80 K).

IV. THERMAL CONDUCTIVITY

In this section, we address the relationship between atomic structure and thermal conductivity (B in Fig. 1), with minimal consideration of the phonon dispersion.

A. Green-Kubo method

The net flow of heat in the MD system, given by the heat current vector **S**, fluctuates about zero at equilibrium. In the GK method, the thermal conductivity is related to how long it takes for these fluctuations to dissipate. For the layered crystal under consideration, the thermal conductivity will be anisotropic (different in the in-plane and cross-plane directions) and for a direction l will given by[30]

$$k_l=\frac{1}{k_B V T^2}\int_0^\infty \langle S_l(t)S_l(0)\rangle dt, \tag{6}$$

where t is time and $\langle S_l(t)S_l(0)\rangle$ is the heat current autocorrelation function (HCACF) for the direction l. The heat current vector for a pair potential is given by[30]

$$\mathbf{S}=\frac{d}{dt}\sum_i E_i\mathbf{r}_i=\sum_i E_i\mathbf{v}_i+\frac{1}{2}\sum_i\sum_{j\neq i}(\mathbf{F}_{ij}\cdot\mathbf{v}_i)\mathbf{r}_{ij}, \tag{7}$$

where E_i, $\mathbf{r}_i$, and $\mathbf{v}_i$ are the energy, position vector, and velocity vector of particle i, and $\mathbf{r}_{ij}$ and $\mathbf{F}_{ij}$ are the interparticle separation vector and force vector between particles i and j.

The most significant challenge in the implementation of the GK method is the specification of the integral in Eq. (6), which may not converge due to noise in the data. Such an event may be a result of not obtaining a proper sampling of the system's phase space, even when averaging over a number of long, independent simulations, as we have done here. Thus, it is not always possible to directly specify the thermal conductivity. As such, we also consider finding the thermal conductivity by fitting the HCACF to a set of algebraic functions.

It has been shown[22,31] that the thermal conductivities of the monatomic LJ fcc crystal and a family of complex silica structures can be decomposed into contributions from short and long time-scale interactions by fitting the HCACF to a function of the form

$$\langle S_l(t)S_l(0)\rangle=\mathrm{A}_{ac,sh,l}\exp\left(\frac{-t}{\tau_{ac,sh,l}}\right)+\mathrm{A}_{ac,lg,l}\exp\left(\frac{-t}{\tau_{ac,lg,l}}\right)+\sum_j \mathrm{B}_{op,j,l}\exp\left(\frac{-t}{\tau_{op,j,l}}\right)\cos(\omega_{op,j,l}t). \tag{8}$$

Here, the subscripts *sh* and *lg* refer to short-range and long-range, the A and B parameters are constants, and τ denotes a time constant. The summation in the optical phonon term corresponds to the peaks in the Fourier transform of the HCACF,[31] where $\omega_{op,j,l}$ is the frequency of the jth peak in the lth direction. This term is used when appropriate (i.e., for crystals with more than one atom in the unit cell). Substituting Eq. (8) into Eq. (6),

$$k_l=\frac{1}{k_B V T^2}\left(\mathrm{A}_{ac,sh,l}\tau_{ac,sh,l}+\mathrm{A}_{ac,lg,l}\tau_{ac,lg,l}+\sum_j\frac{\mathrm{B}_{op,j,l}\tau_{op,j,l}}{1+\tau_{op,j,l}^2\omega_{op,j,l}^2}\right)\equiv k_{ac,sh,l}+k_{ac,lg,l}+k_{op,l}. \tag{9}$$

Further details on the decomposition can be found elsewhere.[22,31] In this investigation, a fit of Eq. (8) was possible for all cases except the cross-plane direction for (i) $R_m=5$ ($T\geqslant 60$ K) and (ii) $R_m=10$ ($T\geqslant 40$ K). In these cases, the peak in the spectrum of the HCACF broadens to the point where it is no longer well represented by an exponentially decaying cosine function in the time coordinate.[32] The agreement between the fit thermal conductivity and that specified directly from the integral is generally within 10%. When available, the fit values are reported.

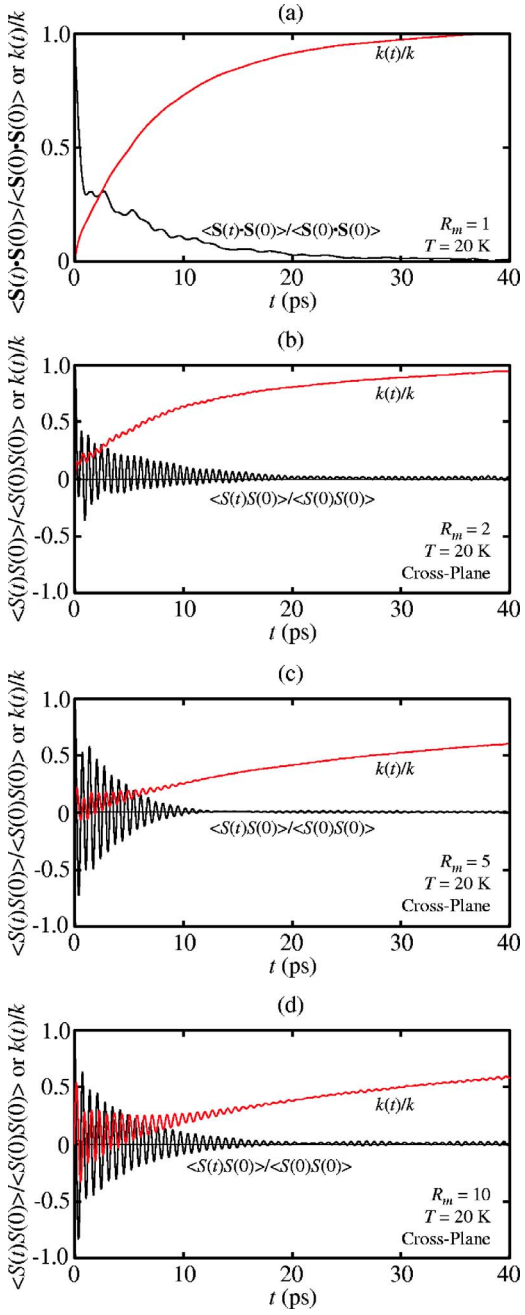

FIG. 5. (Color online) The HCACF (black line) and its integral [red (gray) line, whose converged value is the thermal conductivity] for R_m= (a) 1, (b) 2, (c) 5, and (d) 10 at a temperature of 20 K. The data for the latter three cases correspond to the cross-plane direction. The HCACF is scaled against the zero time value, whereas the thermal conductivity is scaled against its converged long-time value.

B. Heat current autocorrelation function

The time dependence of the HCACF (normalized by its zero-time value) and its integral (the thermal conductivity, normalized by its converged value) are plotted for four cases at a temperature of 20 K in Figs. 5(a)–5(d).

The data in Fig. 5(a) correspond to the monatomic system. The HCACF decays monotonically (small oscillations

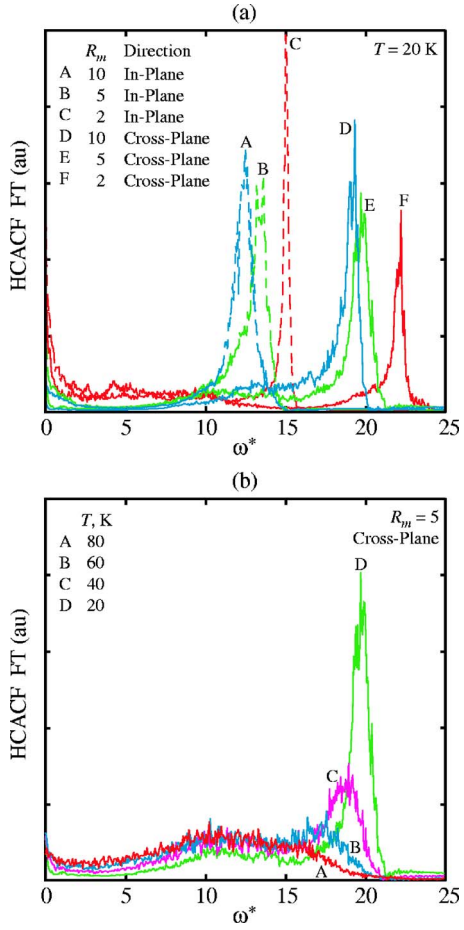

FIG. 6. (Color online) HCACF frequency spectra for (a) T =20 K, mass ratios of 2, 5, and 10 in both the in-plane and cross-plane directions and (b) mass ratio of 5, cross-plane direction, for temperatures of 20, 40, 60, and 80 K.

can be attributed to the periodic boundary conditions[26]), and is well fit by the sum of two decaying exponentials [the first two terms in Eq. (8)]. Such behavior is found at all temperatures considered for the monatomic system.

The data in Figs. 5(b)–5(d) correspond to the cross-plane direction for R_m values of 2, 5, and 10. Significant oscillations in the HCACF are present and grow as the mass ratio is increased. This is the effect of the optical phonon modes.[31] The HCACF can be fit by Eq. (8), with one term taken in the optical summation (this is justified by the HCACF spectra shown later). The integrals in Figs. 5(c) and 5(d) converge at a longer time than shown in the plot. This result indicates that while the oscillations in the HCACF dominate its magnitude, the contribution of the $k_{ac,lg}$ term to the thermal conductivity is significant, even if it cannot be visually resolved. The plots in Fig. 5 show the effect of changing the mass ratio at a fixed temperature. For a fixed mass ratio, increasing the temperature leads to a HCACF that decays faster. Fewer periods are captured in the decay, which makes it harder to extract the oscillation frequency. Results for the in-plane direction are qualitatively similar.

In Fig. 6(a), the Fourier transform (FT) of the normalized HCACF is plotted for mass ratios of 2, 5, and 10 in the in-plane and cross-plane directions at a temperature of 20 K.

Each of the spectra have a nonzero zero-frequency intercept, and a strong, single peak. This is in contrast to the FT of the monatomic system, which decays monotonically from the zero-frequency value.[22] The peaks fall within the range of the optical phonons. As the mass ratio increases, the location of the peak frequency in each of the directions decreases, which is consistent with the trends in the dispersion curves plotted in Fig. 4(a).

In Fig. 6(b), the FT of the normalized HCACF for a mass ratio of 5 in the cross-plane direction is plotted at temperatures of 20, 40, 60, and 80 K. As the temperature increases, the peak frequency decreases, consistent with the discussion of the effects of temperature on phonon frequencies in Sec. III. The peak also broadens considerably, and its magnitude decreases; the behavior is better described as broadband excitation. It is this behavior that leads to the failure of the fitting procedure under certain conditions. This broadening is not as significant for a mass ratio of 2. The origin of the peaks will be further discussed in Sec. V A.

C. Predictions

The thermal conductivities predicted for the $R_m=2$ system are plotted in Fig. 7(a) along with the data for the monatomic unit cell. Also included in the plot are the predictions for a monatomic cell with all atoms having a mass of 1.5 (i.e., $R_m=1$, $m^*=1.5$, giving the same density as the $R_m=2$ system). These results are obtained by scaling the data from the ($R_m=1$, $m^*=1$) system. Although increasing the density lowers the thermal conductivity, the presence of the different masses has a more pronounced effect for both the in-plane and cross-plane directions, with the latter being lower than the former. The thermal conductivities for all cases considered in the cross-plane direction are plotted in Fig. 7(b). The data in Figs. 7(a) and 7(b) are fit with power-law functions to guide the eye. Because of the classical nature of the simulations, all the curves will go to infinity at zero temperature (unlike experimental data, which peaks and then goes to zero at zero temperature).

By considering the LJ thermal conductivity scale, $k_B/\sigma_{LJ}^2(\epsilon_{LJ}/m_{LJ})^{1/2}$, it can be deduced that the thermal conductivity of a monatomic system where each atom has mass m^* is proportional to $(m^*)^{-1/2}$. We will denote the $k \propto (m^*)^{-1/2}$ behavior as the density trend. In Figs. 8(a) and 8(b), the thermal conductivities for mass ratios between 0.1 and 10 in both directions at temperatures of 10, 40, and 70 K are plotted as a function of the average dimensionless atomic mass in the unit cell, $\bar{m}^*$, given by

$$\bar{m}^* = \frac{m_1^* + m_2^*}{2}, \tag{10}$$

which is proportional to the system density. Also plotted for each data series in Figs. 8(a) and 8(b) is the thermal conductivity that would exist in an equivalent monatomic crystal where all atoms have mass $\bar{m}^*$ (i.e., $m^*=\bar{m}^*$). These are the solid lines in the plots, obtained by scaling the ($R_m=1$, $m^*=1$) data point. The dashed lines in Figs. 8(a) and 8(b) correspond to $k \propto (m^*)^{-1/2}$, and have been placed by eye to highlight trends. From these two plots, the relationships between

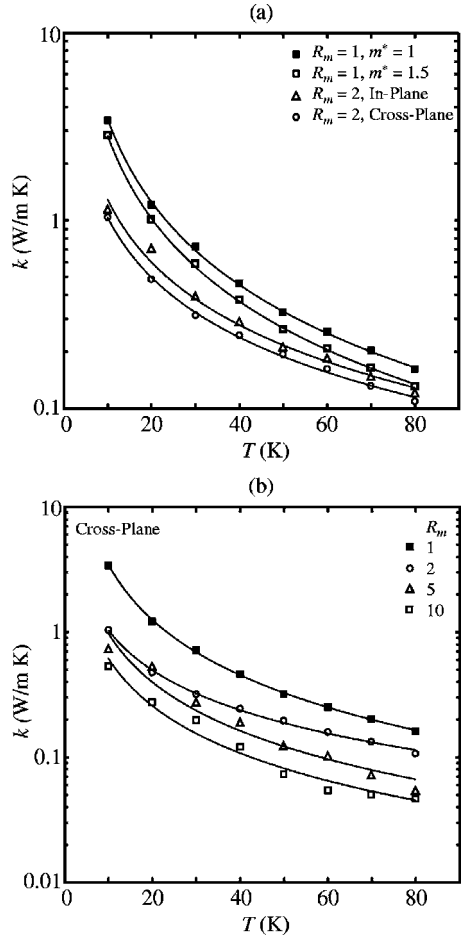

FIG. 7. (a) Thermal conductivity plotted as a function of temperature for mass ratios of 1 and 2. (b) Thermal conductivity in the cross-plane direction plotted as a function of temperature for mass ratios of 1, 2, 5, and 10. The data in both (a) and (b) are fit with power-law functions to guide the eye.

the effects of temperature (i.e., anharmonicity and scattering), density, and the mass ratio become apparent.

In the in-plane direction [Fig. 8(a)], the thermal conductivity data converge toward the same density monatomic system curve as the temperature is increased. At the high temperatures, the mass difference plays no appreciable role, and the thermal conductivity only depends on density. At the lowest temperature, 10 K, the thermal conductivity data do not approach the monatomic value, but do show the density-predicted trend at the large and small mass ratios. This difference between the low- and high-temperature behaviors is due to the difference in the degree of scattering. At high temperatures, the anharmonic effects are strong and tend to override the structural effects.

In the cross-plane direction, the data are never close to the same-density monatomic system, other than at $R_m=1$. At the two low temperatures, the data follow the density trend closely, but with values lower than the monatomic system (this is a structural effect). At the high temperature, 70 K, there is an increase toward and decrease away from the $R_m=1$ thermal conductivity value for increasing mass ratio. Here, we hypothesize that the effect of the increasing density

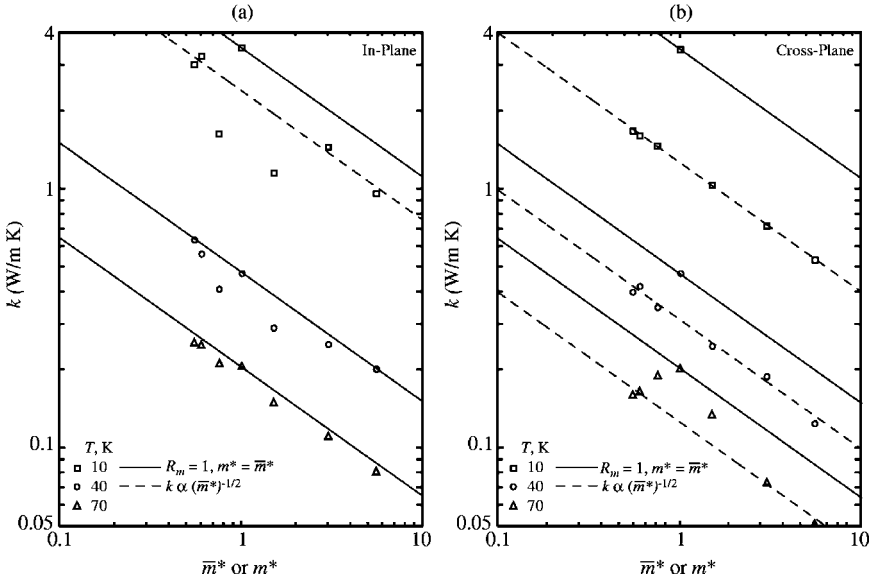

FIG. 8. Thermal conductivity at temperatures of 10, 40, and 70 K in the (a) in-plane and (b) cross-plane directions plotted as a function of the average atomic mass in the system. Also plotted is the thermal conductivity of the equivalent monatomic systems where each atom has a mass $\bar{m}^*$ (solid line). The dashed lines correspond to $k \propto (\bar{m}^*)^{-1/2}$ and are fit to the data by visual inspection.

is offset by the decrease in phonon scattering in the cross-plane direction as the two masses in the system approach the same value.

The general trends in the in-plane and cross-plane directions are different: in the in-plane direction, higher temperature leads to the density trend and apparent structure independence, whereas in the cross-plane direction, the density trend is found at lower temperatures where structural effects are important. Although this difference is most likely a result of the anisotropic nature of the system, the underlying reasons are not yet clear. Qualitatively, a thermal conductivity following the density trend suggests strong contributions from phonon modes in which the atoms in the unit cell move cooperatively—a characteristic of the acoustic phonon modes. In general, from these results we see that having a polyatomic structure introduces additional decreases in thermal conductivity beyond that predicted by density trends.

V. CORRELATION BETWEEN PHONON BAND STRUCTURE AND THERMAL CONDUCTIVITY

In this section, we address the link between thermal conductivity and phonon dispersion (C and C* in Fig. 1), without explicit consideration of the atomic structure.

A. Dispersion and HCACF

Although peaks in the spectrum of the HCACF have been observed,[8,25,31] no comprehensive explanation has been given for their origin. It has been hypothesized that they corresponded to optical phonons[31,33] due to their frequencies lying in that region of the phonon spectrum. Such a result is shown in Fig. 9(a), where the quasi-harmonic phonon dispersion curves for the in-plane direction are shown on top of the HCACF spectra for the in-plane and cross-plane directions for $R_m=2$ and a temperature of 20 K. In Fig. 9(b), the location of the peak [as found in the decomposition of the HCACF with Eq. (8)] is plotted as discrete data points as a function of temperature for the in-plane and cross-plane directions in the $R_m=2$ system. The corresponding data for $R_m=5$ are plotted in Fig. 9(c).

By overlaying the dispersion curves and the HCACF spectra for both directions for a range of temperatures and mass ratios, we find that the peak in the in-plane spectrum is coincident with one of the dispersion branches at zero wave vector (i.e., the Γ point—the center of the Brillouin zone). The associated quasi-harmonic frequency is denoted by ω_2^* in Fig. 9(a) and plotted as a continuous line in Figs. 9(b) and 9(c). A similar coincidence exists for the cross-plane peak, which is consistently near the Γ-point frequency ω_1^*, also shown in Fig. 9(a). These frequencies are also plotted in Figs. 9(b) and 9(c). The link between HCACF peaks and Γ-point frequencies has also been found in LJ superlattice structures with longer period lengths.[34]

The agreement between the HCACF peaks and the dispersion frequencies is very good, especially for the in-plane peak. The data for $R_m=10$ show a similar agreement as for $R_m=5$. The specification of the peak from the HCACF decomposition becomes difficult at high temperatures, particularly in the cross-plane direction [this can be seen in Fig. 6(b)]. Quasi-harmonic theory will lead to an underprediction of the dispersion curve frequencies, which is the case for both peaks.

From these results, it is clear that specific optical phonon modes generate the peaks in HCACF. Because these modes do not make a significant contribution to the thermal conductivity, as will be discussed in Sec. V B, we interpret the appearance of peaks in the HCACF as an indication that they are partly responsible for the increased phonon scattering (and lower thermal conductivity) in the diatomic system.

B. Dispersion and thermal conductivity

As seen in Figs. 7(a) and 7(b), the thermal conductivities in the in-plane and cross-plane directions are lower than the monatomic value. The deviation from the monatomic value increases as the mass ratio increases. In the limit of an infinite mass ratio, the thermal conductivity will go to zero. This

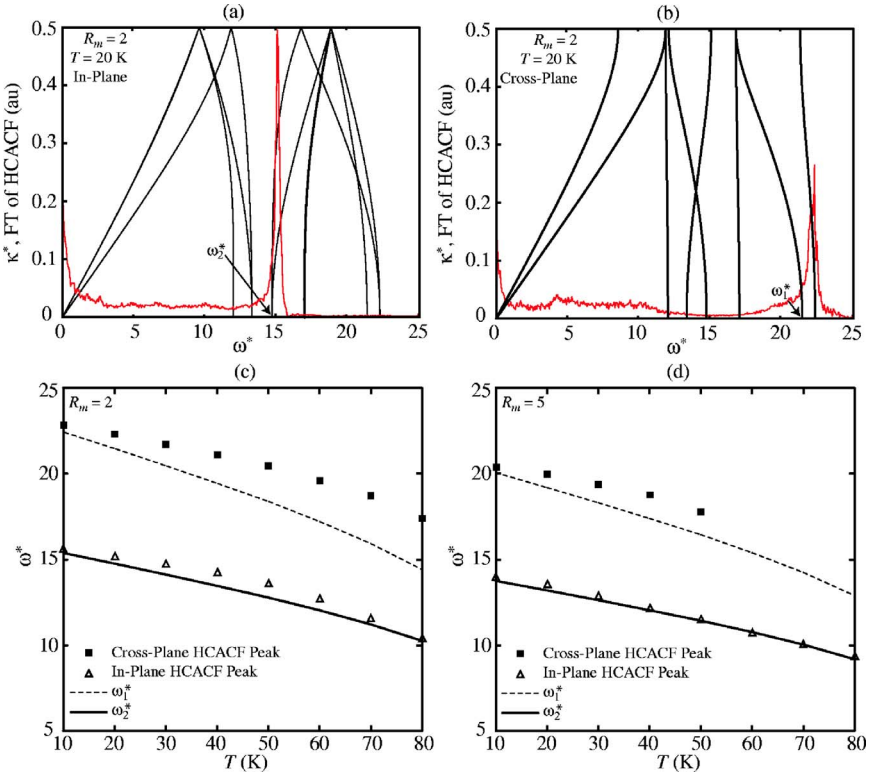

FIG. 9. (Color online) (a) In-plane and (b) cross-plane dispersion curves (black lines) superimposed on the respective HCACF spectra [red (gray) lines] for $R_m = 2$, $T = 20$ K. Comparison of the peaks in the HCACF to the associated frequencies in the quasiharmonic dispersion curves for (c) $R_m = 2$ and (d) $R_m = 5$ in the in-plane and cross-plane directions, plotted as a function of temperature.

limit, and the overall behavior, can be partly understood from the trends in the dispersion curves. As the mass ratio increases, the dispersion branches get flatter (see Fig. 3). The phonon group velocities (related to the slope of the dispersion curves) will get correspondingly smaller until they reach a value of zero when the branches are completely flat, leading to zero thermal conductivity.

It is often assumed, although in most cases not properly justified, that acoustic phonons are the primary energy carriers in a dielectric crystal. Optical phonons are assumed to have a small contribution because of their supposed lower group velocities. Yet from a visual inspection of the dispersion curves in Fig. 3, one can see that there is not a significant difference in the slopes of the acoustic and optical branches. Based on the results of the thermal conductivity decomposition by Eq. (9) (not presented in detail here), the acoustic modes are responsible for most of the thermal conductivity. For a mass ratio of 2 in the cross-plane direction, the acoustic contribution ranges between 99.98% at a temperature of 10 K and 99.79% at a temperature of 80 K. For a mass ratio of 10 in the cross-plane direction, the acoustic contribution ranges between 98.84% at a temperature of 10 K and 85.08% at a temperature of 80 K. Thus, the dispersion trends alone cannot completely explain the observed behavior, and changes in the phonon scattering behavior must be considered.

In Figs. 10(a) and 10(b), the thermal conductivities for all cases considered in this study are plotted as a function of the dispersion metrics p_{ac}, p_{op}, and s_{tot} introduced in Sec. III and plotted in Fig. 4(b). These quantities represent the fraction of the frequency spectrum taken up by the acoustic phonon modes, the optical phonon modes, and the stop bands. All thermal conductivities are scaled by the corresponding $R_m = 1$ value at the same temperature.

From these plots, a number of general trends can be discerned. First, in both the in-plane and cross-plane directions, as the relative extent of the acoustic phonon modes increases, the thermal conductivity increases. As discussed, the acoustic modes are most responsible for the thermal conductivity. A larger frequency extent will lead to larger acoustic phonon group velocities, and a higher thermal conductivity. As the extent of the stop bands increases, the thermal conductivity decreases in both directions. In a stop band, there is no phonon wave propagation and, hence, no means for thermal transport. The optical phonon effect is different in the two directions, consistent with the behavior of p_{op} seen in Fig. 4(b). Initially, in both directions, an increase in p_{op} leads to a decrease in the thermal conductivity. The effect of the optical branches is similar to the effect of the stop bands: an accompanying decrease in the extent of the acoustic phonon modes. This trend continues for the in-plane direction, but the cross-plane direction shows a different behavior, with a decrease in p_{op} as the thermal conductivity decreases. This change of behavior motivates further research on the role of the optical modes, but at least indicates that considering only one of p_{ac}, p_{op}, or s_{tot} is not sufficient, and that all must be considered to completely understand the behavior of a given system.

These results can also shed light on the competition between dispersion characteristics and anharmonic scattering in affecting thermal conductivity. In a harmonic system, energy transport can be completely described by the dispersion curves, as there are no mode interactions. As anharmonicity is introduced to such a system (e.g., by increasing the temperature), the dispersion curves will no longer be sufficient to predict the transport as the modes will interact. From Figs. 10(a) and 10(b), we see that as the temperature increases, the thermal conductivity is less sensitive to changes in the dis-

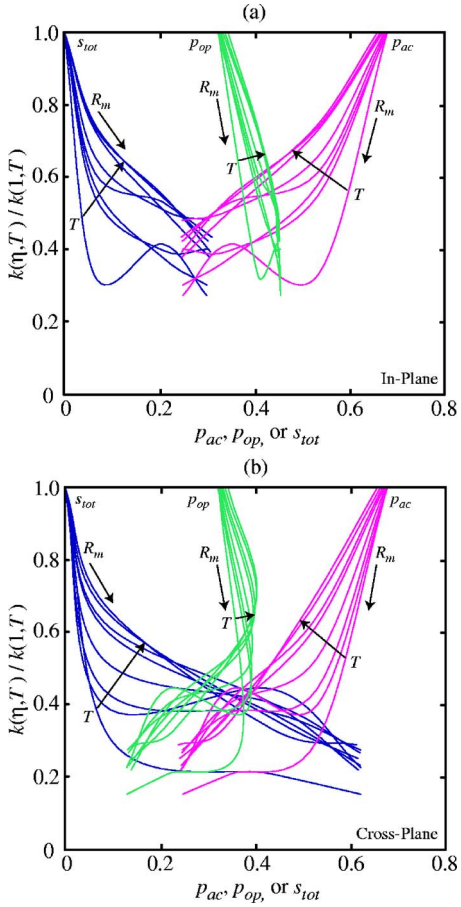

FIG. 10. (Color online) Thermal conductivity at all temperatures and mass ratios considered, scaled by the appropriate $R_m=1$ value, plotted against the phonon dispersion metrics p_{ac} [pink (light gray) lines], p_{op} [green (medium gray) lines], and s_{tot} [blue (dark gray) lines]. To best see the trends, smooth curves through each of the data sets are plotted.

persion metrics (i.e., the magnitude of the slopes of the curves decrease), consistent with the above discussion.

The analysis in this study suggests that a spectral perspective to thermal transport, quantified by dispersion metrics, such as those proposed, provides the following benefits: (i) it enables a quantitative analysis (e.g., by evaluating the slopes of the thermal conductivity vs dispersion metrics curves) of the relative contributions of dispersion and anharmonic scattering mechanisms to thermal transport, and (ii) it uncouples the structure-property relation (as discussed in Sec. IV) to that of structure-dispersion and dispersion-property relations, providing a simplified analysis framework that could be taken advantage of in design studies.

VI. CONCLUSIONS

We have studied a layered diatomic LJ crystal with varying mass ratio in order to establish a temperature-dependent three-way correlation between (i) the unit cell structure and interatomic potential, (ii) the associated phonon dispersion curves, and (iii) the bulk thermal conductivity (see Fig. 1). The dispersion curves were obtained using lattice dynamics calculations, and their characteristics were quantified using a set of band diagram metrics. The thermal conductivity was predicted using molecular dynamics simulations and the GK method.

As shown in Fig. 7, the thermal conductivity of the layered material is less than that of a corresponding monatomic system and is directionally dependent. To understand the thermal conductivity trends, one must consider the effects of density and crystal structure, with consideration to both the dispersion and the anharmonic scattering characteristics (see Fig. 8).

The HCACF for each material was fit to an algebraic function, allowing for the roles of acoustic and optical phonons to be distinguished. The peaks in the FT of the HCACF were found to coincide with frequencies obtained from the dispersion calculations, confirming that these peaks are generated by optical phonons (see Fig. 9).

The dispersion-curve metrics introduced in Sec. III, and plotted in Fig. 4, describe the frequency extent of the acoustic and optical phonon modes and that of the stop bands. As shown in Fig. 10, the thermal conductivity increases with increasing p_{ac}, and decreases with increasing s_{tot}. The dependence on p_{op} varies depending on the mass ratio and the crystallographic direction, a behavior that motivates further investigation.

The rate of change of the thermal conductivity vs the dispersion metrics (see Fig. 10) decreases with increasing temperature, consistent with the increasing role of anharmonic scattering on thermal transport at higher temperature. These relations provide an indirect measure of the relative contributions of dispersion and anharmonic scattering to thermal transport. Moreover, the dispersion metrics allow for the uncoupling of the traditional thermal conductivity structure-property relation to that of structure-dispersion and dispersion-property relations. This decomposition facilitates further elucidation of the underlying physics of thermal transport and could be used as an effective tool for material design.

ACKNOWLEDGMENTS

This work was partially supported by the U.S. Department of Energy, Office of Basic Energy Sciences under Grant No. DE-FG02-00ER45851 (A.J.H.M. and M.K.), and the Horace H. Rackham School of Graduate Studies at the University of Michigan (A.J.H.M.). Some of the computer simulations were performed using the facilities of S. R. Phillpot and S. B. Sinnott in the Materials Science and Engineering Department at the University of Florida.

APPENDIX: LATTICE DYNAMICS CALCULATIONS

In this appendix, we outline the analytical procedure used to investigate the lattice dynamics. The formulation is based on that presented by Dove[27] and Maradudin.[35]

Determining phonon mode frequencies and polarization vectors using lattice dynamics is greatly simplified under the harmonic approximation. In this approximation, a Taylor series expansion of the system potential energy about its mini-

mum value is truncated after the second-order term. This approach leads to harmonic equations of motion that can be solved analytically for simple systems,[28] but are most easily solved numerically.

Given an interatomic potential and the equilibrium positions of the atoms in a crystal with an n-atom unit cell, the analysis proceeds as follows.

The equation of motion of the jth atom ($j=1,2,\ldots,n$) in the kth unit cell is

$$m_j\ddot{\mathbf{u}}(jk,t) = \sum_{j'k'} \mathbf{\Phi}(jk;j'k') \cdot \mathbf{u}(jk,t), \quad \text{(A1)}$$

where m_j is the mass of atom j, $\mathbf{\Phi}$ is the 3×3 force constant matrix describing the interaction between atoms jk and $j'k'$, $\mathbf{u}(jk,t)$ is the displacement of atom jk from its equilibrium position, and the summation is over every atom in the system (including jk itself). The elements of $\mathbf{\Phi}$ are given by

$$\mathbf{\Phi}_{\alpha\beta}(jk;j'k') = \begin{cases} -\chi_{\alpha\beta}(jk;j'k') & jk \neq j'k' \\ \sum_{j''k''} \chi_{\alpha\beta}(jk;j''k'') & jk = j'k', \end{cases} \quad \text{(A2)}$$

where α and β can be the Cartesian coordinates x, y, and z. The summation in Eq. (A2) is over pairings between atom jk and every atom in the system other than itself. For a two-body potential, $\phi(r)$, $\chi_{\alpha\beta}$ is

$$\begin{aligned} &\chi_{\alpha\beta}(jk;j'k') \\ &= \chi_{\alpha\beta}(\mathbf{r}_{jk} - \mathbf{r}_{j'k'}) \\ &= \left.\frac{\partial^2\phi(r)}{\partial r_\alpha \partial r_\beta}\right|_{r=|\mathbf{r}_{jk}-\mathbf{r}_{j'k'}|} \\ &= \left.\left\{\frac{r_\alpha r_\beta}{r^2}\left[\phi''(r) - \frac{1}{r}\phi'(r)\right] + \frac{\delta_{\alpha\beta}}{r}\phi'(r)\right\}\right|_{r=|\mathbf{r}_{jk}-\mathbf{r}_{j'k'}|}, \end{aligned} \quad \text{(A3)}$$

where $'$ indicates a derivative with respect to r, $\delta_{\alpha\beta}$ is the δ function, $\mathbf{r}$ is a position vector, and r_α is the α component of $\mathbf{r}$.

The solution to Eq. (A1) is assumed to be harmonic and is a summation over the normal (phonon) modes of the system, which are traveling waves. Each normal mode has a different wave vector $\boldsymbol{\kappa}$ and dispersion branch ν such that

$$\mathbf{u}(jk,t) = \sum_{\boldsymbol{\kappa},\nu} m_j^{-1/2}\mathbf{e}_j(\boldsymbol{\kappa},\nu)\exp\{i[\boldsymbol{\kappa}\cdot\mathbf{r}(jk) - \omega(\boldsymbol{\kappa},\nu)t]\}, \quad \text{(A4)}$$

where ω is the mode frequency and t is time. The allowed wave vectors are set by the crystal structure. Substituting Eq. (A4) into Eq. (A1) leads to the eigenvalue equation

$$\omega^2(\boldsymbol{\kappa},\nu)\mathbf{e}(\boldsymbol{\kappa},\nu) = \mathbf{D}(\boldsymbol{\kappa})\cdot\mathbf{e}(\boldsymbol{\kappa},\nu), \quad \text{(A5)}$$

where $\mathbf{D}(\boldsymbol{\kappa})$ is the $3n\times 3n$ dynamical matrix and $\mathbf{e}(\boldsymbol{\kappa},\nu)$ is the polarization vector of length $3n$. In Eq. (A4), $\mathbf{e}_j(\boldsymbol{\kappa},\nu)$ contains the three elements of $\mathbf{e}(\boldsymbol{\kappa},\nu)$ that correspond to the jth atom of the unit cell (elements $3j-2$, $3j-1$, and $3j$). The elements of $\mathbf{D}(\boldsymbol{\kappa})$ are given by

$$\begin{aligned} &D_{3(j-1)+\alpha,3(j'-1)+\beta}(jj',\boldsymbol{\kappa}) \\ &= \frac{1}{(m_j m_{j'})^{1/2}}\sum_{k'} \mathbf{\Phi}_{\alpha\beta}(j0;j'k')\exp(i\boldsymbol{\kappa}\cdot[\mathbf{r}(j'k') - \mathbf{r}(j0)]). \end{aligned} \quad \text{(A6)}$$

Here, the summation is over all unit cells and α or β equals 1 for x, 2 for y, and 3 for z. For example, in a unit cell of four atoms denoted by A, B, C, and D (like that shown in Fig. 2), the summation in Eq (A6) for ($j=1$,$j'=2$) would be over pairings between atom A in the zeroth unit cell and atom B in all unit cells, including 0.

The dynamical matrix is Hermitian and therefore has real eigenvalues and orthogonal eigenvectors. The square roots of the eigenvalues of $\mathbf{D}(\boldsymbol{\kappa})$ are the phonon mode frequencies $\omega(\boldsymbol{\kappa},\nu)$, and the eigenvectors of $\mathbf{D}(\boldsymbol{\kappa})$ give the phonon polarization vectors $\mathbf{e}(\boldsymbol{\kappa},\nu)$. The polarization vectors (also known as the mode shapes) are normalized such that

$$[\mathbf{e}(\boldsymbol{\kappa},\nu)]^T\cdot[\mathbf{e}(\boldsymbol{\kappa},\nu)]^* = 1. \quad \text{(A7)}$$

In general, the elements of $\mathbf{e}(\boldsymbol{\kappa},\nu)$ are complex and describe the relative amplitude and phase difference of the displacements of the atoms in the unit cell.

Dispersion curves can be generated by calculating the phonon mode frequencies for a range of wave vectors in a particular direction. For example, the dispersion curve presented in Fig. 3(b) was generated using 100 evenly spaced wave vectors in the in-plane direction with wave numbers ranging from 0 to π/a where a is the lattice constant. The dispersion curve has three acoustic branches and $3n-3$ optical branches. The dispersion shown in Fig. 3(c) has only eight branches because the transverse branches in this direction are degenerate.

The procedure outlined here gives results that are exact at zero temperature. For higher temperatures, the zero-pressure lattice positions should be used (i.e., the quasi-harmonic approximation).[27] The anharmonic contributions to the lattice dynamics analysis can be included using molecular dynamics simulations.[5]

*Present affiliation: Department of Mechanical Engineering, Carnegie Mellon University, Pittsburgh, PA 15213, USA. Electronic address: mcgaughey@cmu.edu

†Present affiliation: Department of Engineering, University of Cambridge, Trumpington Street CB2 1PZ, UK.

[1] In this study, where the phonon transport is diffusive, we will use the term scattering to indicate multiphonon interactions brought about by the anharmonic effects present at finite temperatures.

[2] J. Callaway, Phys. Rev. **113**, 1046 (1959).

[3] M. G. Holland, Phys. Rev. **132**, 2461 (1963).

[4] J. D. Chung, A. J. H. McGaughey, and M. Kaviany, J. Heat Transfer **126**, 376 (2004).

[5] A. J. H. McGaughey and M. Kaviany, Phys. Rev. B **69**, 094303 (2004).

[6] S. Mazumder and A. Majumdar, J. Heat Transfer **123**, 749 (2001).

[7] N. Mingo, Phys. Rev. B **68**, 113308 (2003).

[8] J. Dong, O. F. Sankey, and C. W. Myles, Phys. Rev. Lett. **86**, 2361 (2001).

[9] G. S. Nolas, J. L. Cohn, G. A. Slack, and S. B. Schujman, Appl. Phys. Lett. **73**, 178 (1998).

[10] J. L. Cohn, G. S. Nolas, V. Fessatidis, T. H. Metcalf, and G. A. Slack, Phys. Rev. Lett. **82**, 779 (1999).

[11] D. A. Broido and T. L. Reinecke, Phys. Rev. B **70**, 081310(R) (2004).

[12] M. V. Simkin and G. D. Mahan, Phys. Rev. Lett. **84**, 927 (2000).

[13] Y. Chen, D. Li, J. R. Lukes, Z. Ni, and M. Chen, Phys. Rev. B **72**, 174302 (2005).

[14] Y. Chen, D. Li, J. Yang, Y. Wu, J. R. Lukes, and A. Majumdar, Physica B **349**, 270 (2004).

[15] R. Venkatasubramanian, Phys. Rev. B **61**, 3091 (2000).

[16] S. Chakraborty, C. A. Kleint, A. Heinrich, C. M. Schneider, J. Schumann, M. Falke, and S. Teichert, Appl. Phys. Lett. **83**, 4184 (2003).

[17] J. C. Caylor, K. Coonley, J. Stuart, T. Colpitts, and R. Venkatasubramanian, Appl. Phys. Lett. **87**, 023105 (2005).

[18] J. Lukes, D. Y. Li, X.-G. Liang, and C.-L. Tien, J. Heat Transfer **122**, 536 (2000).

[19] A. R. Abramson, C.-L. Tien, and A. Majumdar, J. Heat Transfer **124**, 963 (2002).

[20] P. Chantrenne and J.-L. Barrat, J. Heat Transfer **126**, 577 (2004).

[21] J. Lukes and C.-L. Tien, Microscale Thermophys. Eng. **8**, 341 (2004).

[22] A. J. H. McGaughey and M. Kaviany, Int. J. Heat Mass Transfer **47**, 1783 (2004).

[23] A. J. H. McGaughey and M. Kaviany, Phys. Rev. B **71**, 184305 (2005).

[24] N. W. Ashcroft and N. D. Mermin, *Solid State Physics* (Saunders College Publishing, Fort Worth, 1976).

[25] J. Che, T. Cagin, W. Deng, and W. A. Goddard III, J. Chem. Phys. **113**, 6888 (2000).

[26] A. J. H. McGaughey, Ph.D. thesis, University of Michigan, Ann Arbor, MI, 2004.

[27] M. T. Dove, *Introduction to Lattice Dynamics* (Cambridge, London, England, 1993).

[28] C. Kittel, *Introduction to Solid State Physics*, 7th ed. (Wiley, New York, 1996).

[29] M. I. Hussein, K. Hamza, G. M. Hulbert, R. A. Scott, and K. Saitou, Struct. Multidiscip. Optim. **31**, 60 (2006).

[30] D. A. McQuarrie, *Statistical Mechanics* (University Science Books, Sausalito, 2000).

[31] A. J. H. McGaughey and M. Kaviany, Int. J. Heat Mass Transfer **47**, 1799 (2004).

[32] This unsuitability of the fitting procedure in these eight cases (out of 64 total) was not found in an investigation of silica structures.[31] In that case, all the peaks remained well-defined over the temperature range considered and did not interfere with the low-frequency behavior. There are two likely explanations for the findings here. First, the mass ratio in silica structures, $m_{Si}/m_O \simeq 28/16 = 1.75$, is much smaller than the mass ratios where we encounter difficulties. Second, the LJ simulations are being run at temperatures close to their melting temperatures (87 K for the monatomic system), whereas the silica simulations were run between temperatures of 100 and 350 K, well below the melting temperatures, which are >1000 K.

[33] P. J. D. Lindan and M. J. Gillan, J. Phys.: Condens. Matter **3**, 3929 (1991).

[34] E. S. Landry, A. J. H. McGaughey, and M. I. Hussein, *Proceedings of the ASME International Mechanical Engineering Conference and Exposition*, Chicago (ASME, New York, 2006), ASME Paper No. IMECE2006-13673.

[35] A. A. Maradudin, in *Dynamical Properties of Solids*, edited by G. K. Horton and A. A. Maradudin (Elsevier, New York, 1974), Vol. 1, pp. 1–82.